REDUCING A FLUCTUATION IN BURST FIRING OF A SQUARE-WAVE BURSTER SILICON NEURON MODEL

Takashi Kohno
Institute of Industrial Science
University of Tokyo
Japan
kohno@sat.t.u-tokyo.ac.jp

Kazuyuki Aihara
Institute of Industrial Science
University of Tokyo
Japan
aihara@sat.t.u-tokyo.ac.jp

Abstract

The silicon neuron is an electronic circuit that reproduces the electrophysiological behavior of neuronal cells. In experimental results of a square-wave burster silicon neuron circuit, we found a characteristic fluctuation in spike generation in its fast subsystem, which leads to instability in the bursting behavior. This article proposes a biologically possible countermeasure against this problem in the modeling aspect, which is originally intuitive and expanded based on the formalism of the ionic current models. Its qualitative effectiveness is evaluated using our silicon neuron model. To support the possibility that this measure is also effective in biological cells, a simulation was performed with a well-known virtual neuron model.

Key words

Silicon neuron, Square-wave burster, Nonlinear dynamics, Neuron model

1 Introduction

The nerve system receives huge amount of input data, robustly extracts critical information from them, and decides appropriate responses in real time. In addition, learning ability improves the responses dynamically and autonomously. These splendid information processing features are realized by far lower-power consumption and more compact system than the digital computers. The silicon neural network is one of the most promising candidates of the next generation information processing systems that realize these features. It is a network of silicon neurons, electronic copies of neuronal cells, connected each other by silicon synapses. The silicon neuron has a long research history and there have been proposed a number of excellent circuits [Renaud, Tomas, Bornat, Daouzli, and Saïghi, 2007; Simoni, Cymbalyuk, Sorensen, Calabrese, and DeWeerth, 2004; Indiveri, 2003]. However, because most of them have been designed to solve neuron models utilizing analog electronic circuit, they are extremely complex and consume larger resources and higher power if the model is detailed whereas their dynamics are restricted if ultimately simplified models such as the leaky integrate-and-fire model are selected.

We proposed a mathematical-structure-based designing approach based on the qualitative modeling techniques of the ionic conductance dynamics in neuronal cells [Kohno and Aihara, 2008; Kohno and Aihara, 2010]. These techniques allow us to describe the mechanisms of the dynamics by fewer system variables and simpler equations than the conductance-based models. In our designing approach, silicon neuron models are constructed by a combination of the characteristics curves of simple, compact, and low-power consuming elemental circuits instead of polynomials that are most tractable in mathematics. Our most recent very-large-scale integrated circuit (VLSI) chip contains a square-wave burster silicon neuron circuit. The square-wave burster [Wang and Rinzel, 2003] is a class of bursters with most simple dynamics, that is composed of a fast subsystem with bistability between a limit cycle and an equilibrium, and a slow negative feedback on it. The Hindmarsh-Rose model [Hindmarsh and Rose, 1984], a pacemaker neuron model in the pre-Bötzinger complex [Butera, Rinzel, and Smith, 1999], and the pancreas β cell model [Chay, 1996] belong to this class. In circuit experiments, we found that the burst firing patterns in our silicon neuron circuit were hard to be stabilized though circuit simulation under noiseless condition concluded stable burst firing. Apparently this instability is attributable to the internal noise of the circuit. Because it is impossible to eliminate noises in real-world systems, our silicon neuron requires some mechanisms to reduce this effect of the internal noise as well as improvement of noise resistance of circuitry. In this article, after a brief overview of our silicon neuron model, simulation results are reported on effectiveness of a biologically possible mechanism in our model and a well-known semi-qualitative model based on the Morris-Lecar model [Rinzel and Ermentrout, 1998].

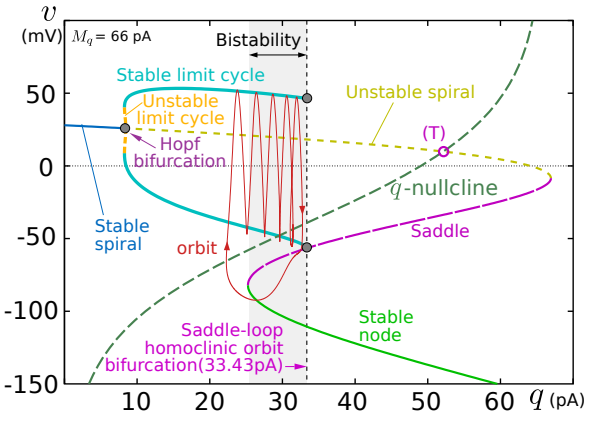

Figure 1. The v-q plane of our silicon neuron model.

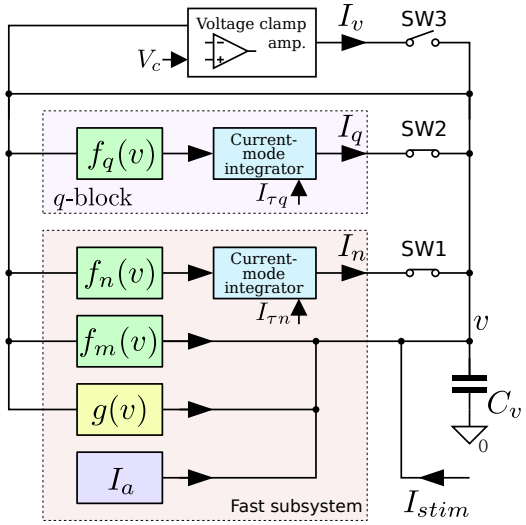

Figure 2. Block diagram of our silicon neuron circuit.

2 A square-wave burster silicon neuron

In the background of our designing approach is the belief that the qualitative properties of the neuronal behaviors, not the exact shape of the action potentials, hold the essences of the nervous information processing. Our silicon neuron circuit is designed based on a theoretical model constructed by a combination of the idealized characteristics curves of the elemental circuitries.

2.1 Model

Our silicon neuron has the minimum number of variables to realize the dynamics in the square-wave burster; a two-variable fast subsystem and a slow feedback variable. The system equations are as follows:

$$C_v \frac{dv}{dt} = -g(v) + f_m(v) - n - q + I_a + I_{\text{stim}}, \quad (1)$$

$$\frac{dn}{dt} = \frac{f_n(v) - n}{T_n}, \quad (2)$$

$$\frac{dq}{dt} = \frac{f_q(v) - q}{T_q}, \quad (3)$$

where variables v and n represent the membrane potential and a hyperpolarizing current that compose the fast subsystem, and q represents the slow hyperpolarizing current that gives a slow negative feedback to it. Parameters C_v, I_a, T_n, and T_q are the membrane capacitance, a constant leak current, the time constants of n and q, respectively. Functions $f_x(v)$ (x=m, n, or q) and $g(v)$ represent the idealized characteristics of most simple, compact and low-power consuming circuits based on the differential pair circuitry composed of Metal-Oxide-Semiconductor Field-Effect Transistors (MOSFETs) operated under the subthreshold condition. They are the similar functions to the hyperbolic tangent as listed in Eqs. (4) and (5). They belong to the most simple, compact, and low-power consuming circuits.

$$f_x(v) = M_x \frac{1}{1 + \exp\left(-\frac{\kappa}{U_T}(v - \delta_x)\right)}, \quad (4)$$

$$g(v) = S \frac{1 - \exp\left(-\frac{\kappa}{U_T}(v - \theta)/2\right)}{1 + \exp\left(-\frac{\kappa}{U_T}(v - \theta)/2\right)}. \quad (5)$$

Here U_T is the thermal voltage (approximately 26mV) and κ is the capacitive-coupling ratio that is dependent on the fabrication process and the operating condition of MOSFETs (between 0.6 and 1.0 in most cases). Parameters M_x, δ_x, S, and θ as well as I_a, T_n, and T_q are to be specified by externally applied voltages.

This model generates burst firing patterns if those parameter values are selected appropriately. As shown in the v-q plane of Fig. 1, a bistability between a limit cycle and an equilibrium exists in an interval of q (gray-colored region in the figure), and the q-nullcline roughly separates the limit cycle and the stable node. Because most part of the limit cycle is above the q-nullcline, q increases while the state point is moving along the limit cycle. It is eliminated by a saddle-loop homoclinic orbit bifurcation when q reaches a critical value and the state point jumps to the unique stable state of the equilibrium. Because the stable node is under the q-nullcline, q decreases until it vanishes by a saddle-node bifurcation and the state point jumps to the limit cycle. The mechanism of the square-wave bursting is the repetition of this process; alternation between the tonic firing (the limit cycle) and the silent (the equilibrium) phases.

2.2 Circuit

Figure 2 illustrates the block diagram of our square-wave burster silicon neuron circuit. The voltage of capacitor C_v represents the membrane potential v. Each

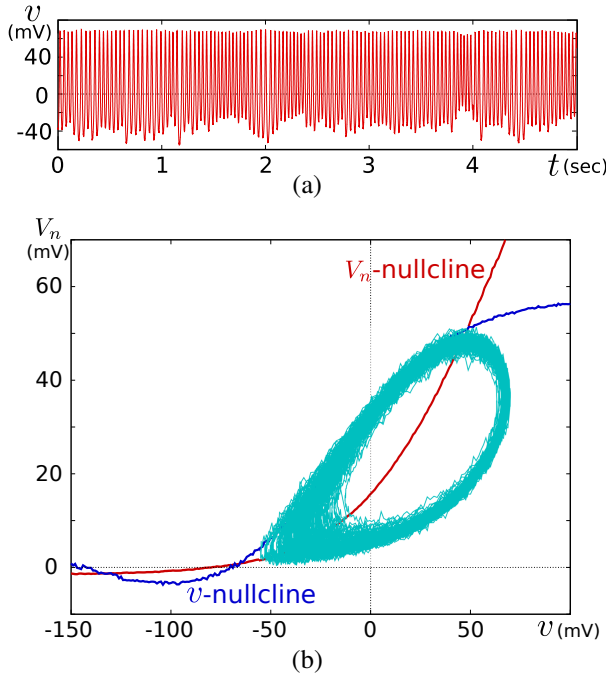

Figure 3. The results of the circuit experiment where q is fixed at a value in the bistability interval. The dimension of n is voltage, because the current that represents n is converted to voltage by a nonlinear high-impedance circuit in the VLSI chip. (a) Time series of v. (b) The same data is projected on the V_n-v phase plane. Variable n is coded by a fine current in the VLSI chip, which is converted to voltage V_n by an integrated I-V converter.

of $f_x(v)$ and $g(v)$ blocks are respectively a differential pair circuit and a transconductance amplifier whose idealized characteristics are represented by Eq. (4) and (5). Their output currents are integrated by the current-mode integrator blocks whose output currents I_q and I_n are integrated in capacitor C_v. The voltage clamp amp. block and switches SW1, 2, and 3 allow us to draw the v-, the n-, and the q-nullclines. How they assist estimating the circuit's dynamics and determining the externally applied parameter voltages, as well as the circuitry of each block, were discussed in our previous works[Kohno and Aihara, 2008; Kohno and Aihara, 2010].

In circuit experiments of our silicon neuron VLSI chips fabricated by TSMC Complementary Metal-Oxide-Semiconductor (CMOS) 0.35μm process, we successfully found the parameter voltages to realize the bistability in the fast subsystem circuit described in the previous subsection and observed bursting behavior. As mentioned in the introduction, however, the bursting behavior could not be stabilized whereas HSPICE circuit simulator concluded stable bursting.

The behavior of the fast subsystem circuit was observed by emulating a fixed value of q by closing SW1, opening SW2 and 3, and applying equivalent I_{stim}. An appropriate selection of I_{stim} value and an initial condition sustains the system state on the limit cycle in the bistability interval of q. In the time course of v (Fig. 3(a)), the lower edge of the oscillation is significantly fluctuating in comparison to the upper edge. Figure 3(b) draws the orbit on the V_n-v phase plane where the experimentally obtained v- and V_n-nullclines are superimposed. In this figure, V_n is a voltage that reflects n, which is originally expressed by a fine current that ranges under 1 nA in our VLSI. The current is converted to a voltage by an internal nonlinear high-impedance circuit to avoid difficulty in measuring dynamical fine currents. Though these nullclines have relatively large errors caused by their measurement circuitries, we can see that the fluctuation is amplified when the system state passes near the saddle point (see Fig. 1 for stability of the equilibria).

3 Possible measures against instability in bursting behavior of silicon neuron model

It is feasible that the fluctuation of v in the fast subsystem reported in the previous subsection originates from the saddle point, because when the state point approaches a saddle point, small displacement of the initial position in the direction along the unstable manifold of the saddle point results significant difference in the orbit. In addition, the q-nullcline is most sensitive to v near the saddle point (see Fig. 1) where this fluctuation is facilitated. There is a possibility that this is one of the crucial mechanisms of the instability in the bursting behavior.

The instability of the bursting behavior that originates from the fluctuation in the fast subsystem is modeled by introducing white noises to v and n in Eqs. (1) and (2) as follows:

$$C\frac{dv}{dt} = -g(v) + f_m(v) - n - q + I_a + I_{\text{stim}} + \xi_v, \tag{6}$$

$$\frac{dn}{dt} = \frac{f_n(v) - n + \xi_n}{T_n}. \tag{7}$$

Figure 4 shows a simulation result of the model of Eqs. (6) and (7) in the similar setting as in Fig. 3 where q is fixed at a value in the bistability interval. In this figure and the following subsections, standard deviation of ξ_v and ξ_n are 2.0×10^{-2} (mV) and 8.0×10^{-5} (nA), respectively. Though quantitatively much modester, they qualitatively reproduce the fluctuation in the fast subsystem. The behavior of our model under the existence of noises in the fast subsystem was simulated by the model of Eqs. (3), (6), and (7). Their parameters are the same as those in Fig. 1 that produces stable 4-spike bursts if no noise is applied. Figure 5(a) is a time course of v in this system. In the figure, 3- and 5-spike bursts are observed as well as 4-spike bursts. The appearance frequencies of N-spike bursts in a 1000 bursts are listed in the "original" column in Table 1. Their average and standard deviation are calculated using 10 trials of the 1000 bursts. In this article, the stability of bursting is evaluated by the spike number per burst instead of the bursting period. This is because it is natural to assume

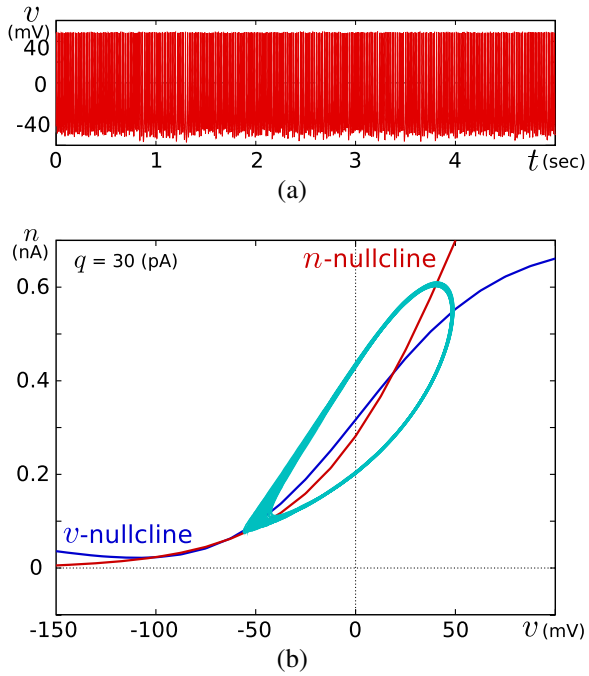

Figure 4. Simulation results of Eqs. (6), (7), and (3) where q is fixed at a value in the bistability interval. (a) Time series of v. (b) The same data is projected on the n-v phase plane.

that the fluctuation in the discrete quantity of the former has more impact on the behavior of the neuronal networks than the variation in the continuous number of the latter. In addition, the stabilization of the former has an effect of reducing variance in the latter.

3.1 Modification of the q-nullcline

The saddle point in the fast subsystem is an inevitable structure in the dynamics of the square-wave burster. Thus, a possible countermeasure against this mechanism in the modeling aspect is to make the fluctuation of v in the limit cycle less effective on $\frac{dq}{dt}$. A most straightforward way to realize this is reducing the sensitivity of the q-nullcline to v near the saddle point. If we redefine sigmoidal function $f_q(v)$ in Eq. (3) as follows, the width of and the gradient of its plateau region can be arranged by constant K.

$$f_q(v) = M_q \frac{1}{1 + \exp\left(-K \frac{\kappa}{U_T}(v - \delta_q)\right)}. \qquad (8)$$

Larger value of K increases the steepness of the sigmoid, which leads to the wider and less gradient plateau region. This $f_q(v)$ is approximately implementable in CMOS circuit.

Figure 6 illustrates the v-q plane of our silicon neuron model with this modification, where the new q-nullcline is steepened (K = 10) and displaced so that the model generates stable 4-spike bursts with similar bursting period to the original setting if no noise is applied. A time course of v is plotted in Fig. 5(b) and the average and the standard deviation of the appearance

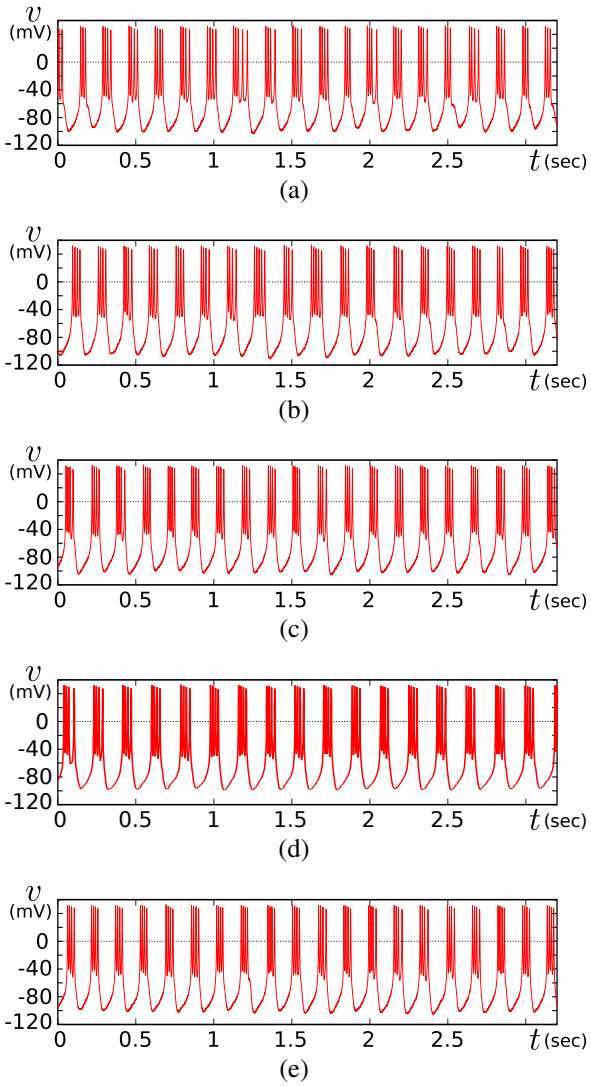

Figure 5. Time courses of v in our silicon neuron model when white noises are applied to v and n. (a) Original model, (b) The q-nullcline is steepened, (c) The dependence of the time constant of q is introduced into (b), (d) The same modification as (c) is applied to (a), (e) White noise ξ_q is introduced to q in (c).

frequencies of N-spike bursts are listed in the "mod.1" column in Table 1. The appearance of 2- and 6-spike bursts are eliminated and 3- and 5-spike bursts are reduced approximately by half.

3.2 Biologically-inspired modification

In the ionic conductance models of the excitable cells, some ionic currents without inactivating dynamics are formulated as follows:

$$I_x = \bar{g_x}\, z^{N_z}\, (E_x - v), \qquad (9)$$

$$\frac{dz}{dt} = F_z(v, z), \qquad (10)$$

where $\bar{g_x}$ represents the maximum conductance of ionic channel x, m is an activating gate variable, and v is the membrane potential. Constant N_z is a positive

Table 1. Appearance frequencies of from 2- to 6-spike bursts in a 1000 bursting. The "N" column represents the number of spikes per burst. Their average and standard deviation are calculated using 10 trials (total 10000 burstings). Each column corresponds to the time-series plot in Fig. 5 from (a) to (e) in sequence, whose condition is described in section 3.

N	original	mod.1	mod.2	mod.3	mod.2 with noise in q
2	0.1 ± 0.32	0	0	0.1 ± 0.32	0
3	226.3 ± 11.91	106.7 ± 7.79	13.9 ± 3.00	25.1 ± 4.91	15.7 ± 4.52
4	718.7 ± 10.91	861.8 ± 8.05	973.5 ± 5.10	968.3 ± 4.88	971.3 ± 5.60
5	54.6 ± 12.55	31.5 ± 5.68	12.6 ± 3.10	6.5 ± 1.72	13.0 ± 3.89
6	0.3 ± 0.67	0	0	0	0

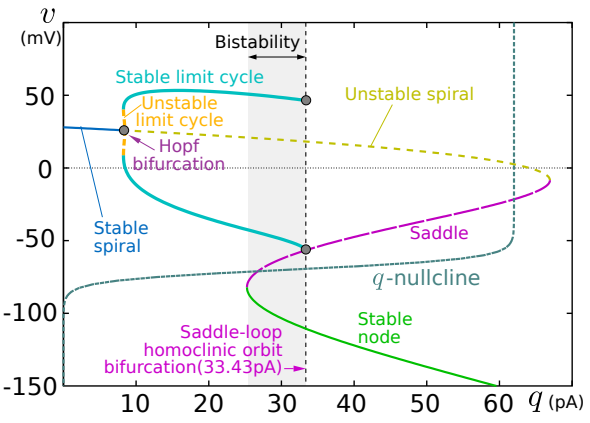

Figure 6. The v-q plane of a modified silicon neuron model. The difference to Fig. 1 is that the q-nullcline is steepened by setting K = 10 and displaced along the v-axis. Under the noise-free condition, the model generates stable 4-spike bursts of very similar bursting period to the original model.

integer and E_x is the equilibrium potential of the ion selected by ionic channel x. In the conductance models, the slow feedback dynamics in the square-wave burster are realized by ionic currents that follow this formalism.

Thus, the modification in the previous subsection corresponds to steepening the I_q-nullcline where I_q is an ionic current that produces the slow feedback dynamics. The equations above indicate that the I_q-nullcline is steeper if larger N_z as well as a steeper z-nullcline is selected. In the case that N_z is larger than 1, the time constant of I_x is proportional to $1/z^{N_z-1}$, which means that the time constant is decreased by increase in z. This accelerates the effect of negative feedback as the system state approaches the saddle-loop homoclinic orbit bifurcation point. Near this bifurcation point, the system state on the stable limit cycle can easily be repelled out of it by the noise because an stable manifold of the saddle point is very close to the limit cycle. It is intuitive that the shorter staying time near the bifurcation point would reduce the noise effect.

This mechanism can be introduced into our silicon neuron model in the previous subsection by changing Eq. (3) to

$$\frac{dq}{dt} = \frac{f_q(v) - q}{T_q / f_T(q)}, \tag{11}$$

where $f_T(q)$ is a monotonic increasing function that is approximately implementable by a relatively simple CMOS circuit. It is

$$f_T(q) = 1 + M_T \frac{1}{1 + \exp\left(-L\frac{\kappa}{U_T}(q - \delta_T)\right)}, \tag{12}$$

where L, M_T, and δ_T are the parameters that are specified by the voltages externally applied to the circuit. Now the modified silicon neuron model is composed of Eqs. (4) (for x=m or n), (5), (6), (7), (8), (11), and (12). Appropriate selection of these three new parameters and re-selection of T_q while maintaining the other parameters the same as in the previous subsection considerably improved the stability of bursting behavior. A time course of v is plotted in Fig. 5(c), where all the numbers of spikes in the bursts are 4 in a relatively short time window. The average and the standard deviation of the appearance frequencies of N-spike bursts are listed in the "mod.2" column in Table 1. The rate of 4-spike burst is increased up to about 97%.

Another plot in Fig. 5(d) is a time series of v in a system obtained by applying the same modification to the original silicon neuron model (non-steep q-nullcline). The system equations are composed of Eqs. (3), (4) (for x=m, n, or q), (5), (6), (7), (11), and (12). Here, the new three parameters are selected and T_q is re-selected appropriately, whereas the other parameters are the same as in the original model. The appearance frequencies of N-spike bursts are listed in the "mod.3" column in Table 1, where we see that the rate of 4-spike burst is similarly high as "mod.2". It implies that the major effect of the modification in this section is attributable to the modification in the time constant of q, not to steepness of the q-nullcline.

3.3 Influence of noise in q

In the simulations above, no noise is applied to the slow feedback variable q. We performed simulations

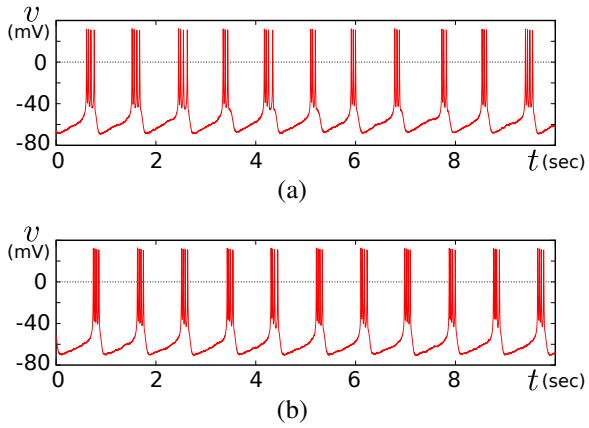

Figure 7. Simulation results of a virtual neuron model. (a) Original model (N_z=1). (b) Modified model (N_z=4).

of the model in the previous subsection under the same condition except for adding white noise ξ_q to q in Eq. (11) in the same way as in Eq. (7). The same value of standard deviation as in ξ_n (8.0×10^{-5} (nA)) is selected for ξ_q. This value seems relatively large if the difference between the scales of variables q and n is taken into account, but it is feasible because both of the variables are implemented in very similar circuitries that have similar intrinsic noises. Figure 5(e) shows a time course of v, where no other than 4-spike bursts is observed as in the result in the previous section. The average and the standard deviation of the appearance frequencies of N-spike bursts were calculated in the same way. They are listed in the rightmost column in Table 1, which has no significant difference to those under the noise-free condition ("mod.2" column). To view how the rhythm of bursting is affected by this noise, the bursting period was evaluated by the interval between the times when v crosses 0 (mV) upward for the first time in a burst and the next. It was 162.3±6.03 (msec) for the simulation result in this subsection whereas 162.3±5.86 (msec) for noise-free q condition in the previous subsection. These values were calculated using the simulation results of the same 10 sets of 1000 bursts for the calculation of appearance frequencies. The increase in the standard deviation of the bursting period by the noise in q is considerably small in comparison to the standard deviation itself.

4 Discussion and Conclusion

We proposed an effective measure against instability in the bursting behavior of a square-wave burster silicon neuron model. It originates from the consideration on the qualitative dynamics in the square-wave burster and was enhanced by the formalism in the conductance models of the biological excitable cells. Accordingly, the influence of the internal noise in biological square-wave bursters can be reduced by the same mechanism.

To support this possibility, in a well-known virtual neuron model based on the Morris-Lecar model [Rinzel and Ermentrout, 1998], we conducted a simulation of

Table 2. Appearance frequencies of from 2- to 7-spike bursts in a 1000 bursting. The numbers in this table are calculated and listed in the same way as in Table 1.

N	N_z=1	N_z=4
2	3.3 ± 1.25	0
3	408.5 ± 9.63	8.6 ± 4.22
4	498.1 ± 11.54	986.2 ± 5.05
5	85.7 ± 8.33	5.2 ± 2.35
6	4.3 ± 2.63	0
7	0.1 ± 0.32	0

increasing N_z (see Eq. (9)) of the slow negative feedback current. In this model, the membrane capacitance C_v is charged or discharged by a very-fast depolarizing current of calcium I_{Ca}, a hyperpolarizing current of potassium I_{K}, and a very-slow hyperpolarizing current of potassium $I_{\mathrm{K\text{-}Ca}}$ as follows:

$$C_v \frac{dv}{dt} = I_{\mathrm{Ca}}(v) + I_{\mathrm{K}} + I_{\mathrm{K\text{-}Ca}} + I_{\mathrm{L}} + I_{\mathrm{stim}}, \qquad (13)$$

where v is the membrane potential, I_{L} is a leak current independent of v, and I_{stim} is an externally applied stimulus current. The very-slow current $I_{\mathrm{K\text{-}Ca}}$ is responsible for the slow feedback dynamics, which follows the formalism of Eq. (9). The fast subsystem is constructed by v and w, the activating gate variable of I_K whose equation is not described here. In this simulation, white noises ξ_v and ξ_w are introduced into these variables in the same way as in our silicon neuron model. The standard deviation of these noises are respectively 0.2 (mV) and 0.002. Originally in this model, N_z is 1 and stable 4-spike bursts are observed under the noise-free condition. We changed N_z to 4 and arranged the other settings of $I_{\mathrm{K\text{-}Ca}}$ so that the model produces stable 4-spike bursts of similar bursting period to the original setting when no noise is applied. Time courses of v in these cases are plotted in Fig. 7. The appearance frequencies of N-spike bursts in the original and the modified setting are listed in the "N_z=1" and the "N_z=4" columns in Table 2, respectively. These values were calculated in the same way as in Table 1. They indicate significant improvement in stability of bursting behavior. Taking its effectiveness into account, we can imagine a possibility that N_z of slow feedback current is large in some biological square-wave bursters whose stability of bursting patterns is critical in surviving.

The evaluation of quantitative effectiveness of the modification in our silicon neuron circuit will be performed in circuit experiments. Simulational work is ineffective because noises in the circuit is dependent on various factors including those which depend on the details of circuit implementation and the operating environment of the VLSI chip.

Acknowledgments

The study was partially supported by JST PRESTO program, a Grant-in-Aid for Young Scientists (A) 19680015 from the Ministry of Education, Culture, Sports, Science, and Technology, the Japanese Government, and the Aihara Project, the FIRST program from JSPS, initiated by CSTP.

References

Butera Jr. R., Rinzel J., Smith J. (1999). Models of Respiratory Rhythm Generation in the Pre-Bötzinger Complex. I. Bursting Pacemaker Neurons. *J. Neurophysiology*, **82**(1), pp. 382–397.

Chay T. (1996). Electrical bursting and luminal calcium oscillation in excitable cell models. *Biological Cybernetics*, **75**(5), pp. 419–431.

Hindmarsh J. and Rose R. (1984). A model of neuronal bursting using three coupled first order differential equations. *Proc. Royal Society B*, **221**(1222), pp. 87–102.

Indiveri G. (2003). A low-power adaptive integrate-and-fire neuron circuit. In *Proc. IEEE Int. Symp. Circuits and Systems* Bangkok, Thailand, May 25-28. pp. 820–823.

Kohno T. and Aihara K., (2008). A design method for analog and digital silicon neurons –Mathematical-model-based method–. *AIP Conf. Proc.*, **1028**, pp. 113–128.

Kohno T. and Aihara K., (2010). A mathematical-structure-based aVLSI silicon neuron model. In *Proc. Int. Symp. on Nonlinear Theory and its Applications* Krakow, Poland, Sept. 5-8. pp. 261–264.

Renaud S., Tomas J., Bornat Y., Daouzli A., and Saïghi S. (2007). Neuromimetic ICs with analog cores: an alternative for simulating spiking neural networks. In *Proc. Int. Symp. Circuits And Systems* New-Orleans, USA, May 27-30. pp. 3355–3358.

Rinzel J. and Ermentrout B., (1998). Analysis of neural excitability and oscillations. In *Methods in Neural Modeling*, MIT Press. Massachusetts. pp. 251–291.

Simoni M., Cymbalyuk G., Sorensen M., Calabrese R., and DeWeerth S. (2004). A multiconductance silicon neuron with biologically matched dynamics. *IEEE Trans. Biomedical Engineering*, **51**(2), pp. 342–354.

Wang X-J. and Rinzel J. (2003). Oscillatory and bursting properties of neurons. In *The Handbook of Brain Theory and Neural Networks*, MIT Press. Massachusetts. pp. 835–840.